EPRG-PRCI-APGA
23rd Joint Technical Meeting
Edinburgh, Scotland
6–10 June 2022

PAPER TITLE: THE EFFECT OF CATHODIC PROTECTION ON NNSCC CRACK GROWTH IN A SIMULATED BURIED PIPELINE DISBONDMENT
PAPER NUMBER: 16

Ali Smith*, Giuliano Malatesta, Serena Colella
Rina Consulting - Centro Sviluppo Materiali, Rome, Italy

Hanns-Georg Schoeneich
Open Grid Europe, Essen, Germany

Paul Roovers
Fluxys, Ghent, Belgium

* presenting author

ABSTRACT

In this work the effect of cathodic protection (CP) on near neutral stress corrosion cracking (NNSCC) has been studied. Laboratory scale crack growth tests have been performed on an API X60 pipe. Pre-cracked tensile specimens were subjected to cyclic loading whilst immersed in a synthetic soil solution. To recreate the field situation, an artificial disbondment was created by means of a Perspex sleeve. Cathodic protection was then applied at the disbondment open mouth position, creating a potential gradient along the specimen length, with negligible current density at the crack site (deep within the disbondment). The crack growth rate was determined for different applied potentials at the open mouth, aiming to evaluate the role of CP i.e. hydrogen, on crack velocity.

The results revealed that low crack growth rates (comparable to tests in air) were observed for samples tested with no CP applied at the open mouth (OCP case). Increasing the CP level at the open mouth led to a remarkable increase in crack growth rate in the distant shielded zone, roughly 20 times higher than that seen in air. The experimental results and modelling work in the present study suggest crack growth was driven by hydrogen (effect of CP at the open mouth) and mechanical fatigue. Hydrogen diffusion calculations supported these results.

A practical model for the crack growth rate was developed from the current experimental data and selected literature data on compact tension specimens. The developed model considered that crack growth rate was driven by the absorbed hydrogen content from corrosion reactions or CP, as well as by mechanical loading effects. The practical model provided good agreement with the experimental data considering a wide range of combined loading factors and potential levels.

DISCLAIMER

circulated to organisations or individuals not authorised to attend the JTM. The Proceedings and the Papers shall be treated as confidential documents and may not be cited in papers or reports except those published under the auspices of EPRG, PRCI or APGA-RSC.

1. INTRODUCTION

Buried gas pipelines may suffer in service from two types of stress corrosion cracking (SCC) i.e., high pH SCC and near neutral SCC (NNSCC). The former involves cracking in concentrated carbonate and bicarbonate solutions in the pH range 9.5 to 12.5. The latter consists of transgranular cracking in more dilute carbonate-bicarbonate environments, containing also small amounts of chloride and sulphate, with pH in the range 5.5 to 8.5 [1]. Whilst high pH SCC has been studied in great detail in the last 50 years, near neutral SCC was first recognized in 1985, and is still actively studied, with the exact mechanisms still under debate [1,2,3]. Near neutral SCC occurs when groundwater comes into contact with the outer pipe surface, through a break in the plastic coating. Colonies of transgranular cracks form in response to the stress in the pipe wall resulting from the pipes internal pressure. Since this pressure may vary with time in actual service conditions, a simple view of stress-corrosion as a mechanically (static) assisted anodic corrosion process, may be complicated by the presence of a cyclic stress, eventually leading to true corrosion fatigue rather than SCC [3]. Furthermore, as gas transmission pipelines are subjected to cathodic protection (CP), hydrogen generation and ingress into the steel may exaggerate NNSCC or even promote hydrogen embrittlement [1,4]. This could be especially a problem, as pipeline operators encountered with NNSCC, may be tempted to increase the CP level to protect against further crack propagation. However increased protection may promote hydrogen generation, thus increasing the risk of further cracking.

Based on these considerations, the EPRG launched project 204, aiming to study the effect of CP on NNSCC propagation. To this end, the field situation was simulated by performing laboratory scale crack growth tests on grade API X60 pipe samples. The crack growth rate was determined for different applied potentials, aiming to evaluate the role of CP and long range hydrogen diffusion on crack velocity.

2. MATERIAL AND EXPERIMENTAL PROCEDURES

2.1. Material for experiments

The material for study was an X60 grade pipe from the early 1970s with wall thickness of 13.4 mm and outer diameter of 914.4 mm. Table 1 below reveals the measured steel chemistry.

C	Mn	Si	Nb	V	Ti	P	S
0.19	1.40	0.38	0.029	0.071	<0.01	0.014	0.013

Table 1 Chemical composition of pipe in wt% with balancing Fe

The above pipe chemistry is a typical chemistry for a pipe from the early 1970s, i.e., hot rolled and normalized, relying on carbon, manganese, and microalloying (V + Nb) for strength.

The actual yield strength was determined to be 444 MPa, in the longitudinal direction. The microstructure parallel to the pipe long axis was examined via optical microscopy following a nital etch.

Figure 1 shows the resulting microstructures.

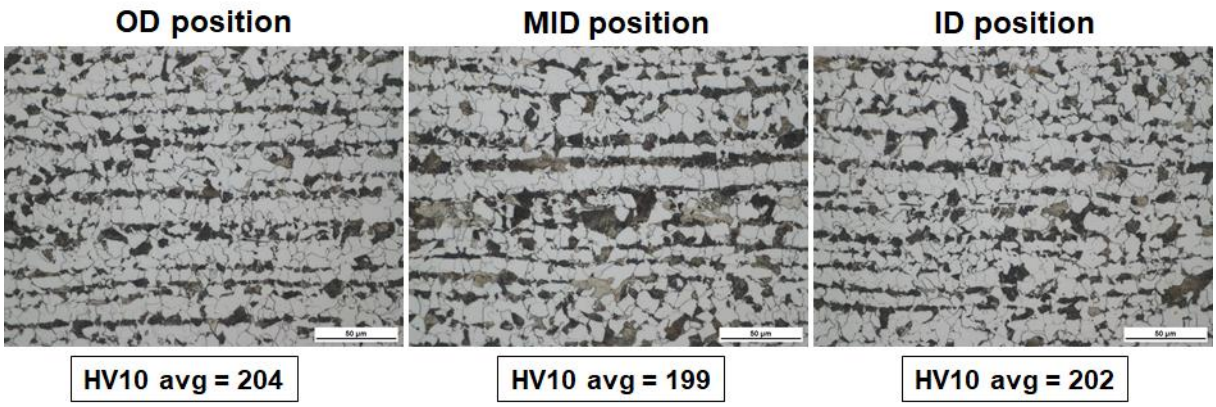

Figure 1 Microstructure and Vickers hardness of the X60 grade pipe through the wall thickness

As can be seen from figure 1, the pipe microstructure exhibits a banded ferrite-pearlite microstructure and uniform hardness throughout the wall thickness. The mid wall position, as expected, reveals a greater intensity of banding.

2.2. Experimental setup

The laboratory crack growth tests were set up to try to recreate the field situation as close as possible. The field scenario of interest is shown via the sketch in figure 2 below.

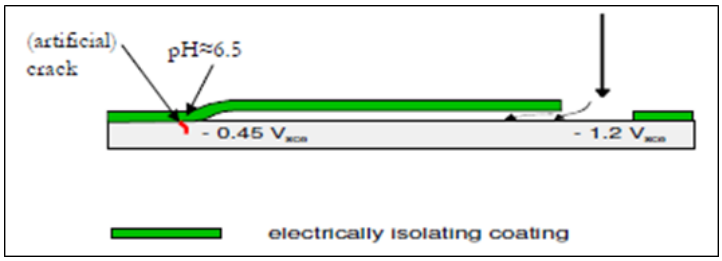

Figure 2 Sketch of pipeline disbondment with NNSCC already present

As can be seen, the bare steel surface is exposed to the surrounding environment (wet soil with dissolved CO_2), via the presence of a disbondment. Deep into the disbondment or crevice, lies a pre-existing NNSCC crack colony. The CP is applied (at the "open mouth") but penetrates only a limited distance inside the disbondment, thus at the crack site there is negligible current density. The lab test should then be set up so that the influence of changing the CP at the "open mouth" on the NNSCC crack growth rate can be understood.

To simulate this field situation an approach inspired by earlier Canadian work was used [5,6]. Thus, to simulate the pipe wall with a preexisting NNSCC short crack, a flat tensile type specimen was used, having an EDM slot machined on one face. This slot gave a semi-elliptical flaw shape with depth a = 2.5 mm and width 2c = 5 mm. The specimens were then pre-cracked in air by fatigue, and epoxy resin coated on all remaining faces. In this way each specimen possessed a reproducible pre-crack, and only one face of the specimen (with pre-cracked notch), was left bare and exposed to the environment.

For the near neutral environment, a synthetic soil solution was used. The composition of this "C2" solution as it is known [5,6], is indicated below, together with the measured conductivity.

Solution	KCl (g/l)	$NaHCO_3$ (g/l)	$CaCl_2.H_2O$ (g/l)	$MgSO_4.7H_2O$ (g/l)	$CaCO_3$ (g/l)	Conductivity (S/m)
C2	0.0035	0.0195	0.0255	0.0274	0.0606	0.0075

Table 2 Composition of synthetic soil solution and electrical conductivity

For the disbonded coating (electrically isolating), a Perspex sleeve or hollow box was constructed.

Figure 3 shows the completed experimental set up.

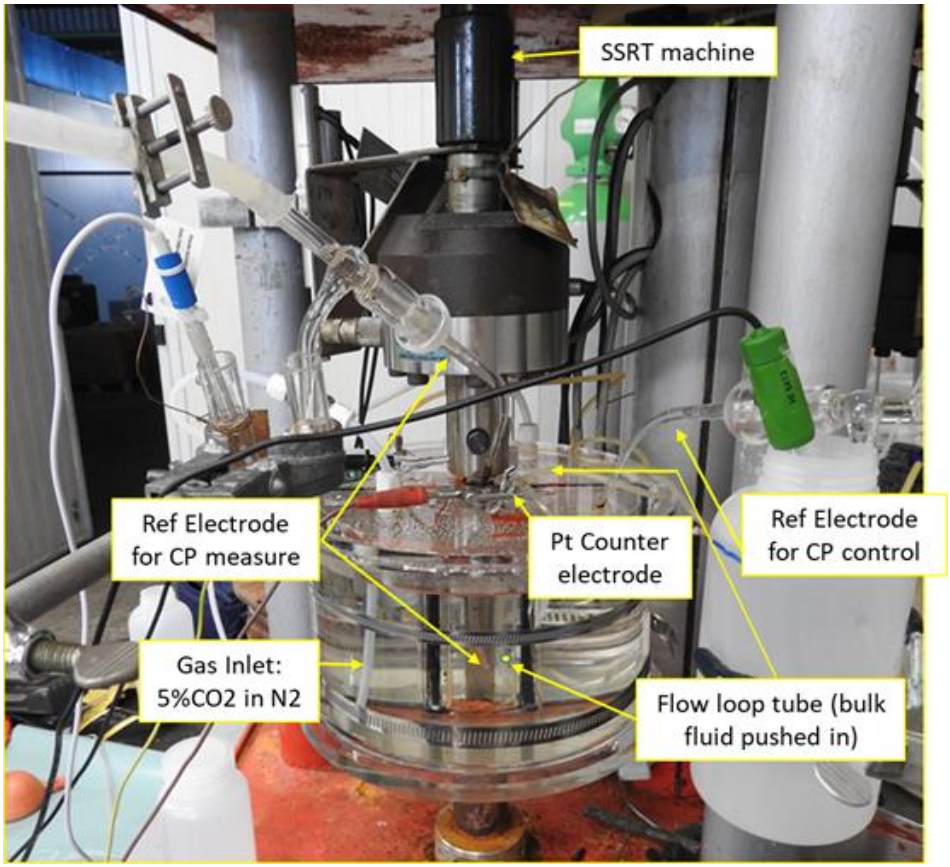

Figure 3 Experimental setup for laboratory crack growth studies

Figure 3 shows the flat tensile specimen attached to the tensile load frame. The specimen is positioned inside a Perspex box open at the top, and around this box is placed the outer chamber. The synthetic soil solution is first de-aerated and saturated with a gas mixture of 5% CO_2 in N_2. The solution is then drawn into the outer chamber to form the bulk solution. The level of liquid is several centimeters above the top of the Perspex box (disbondment). In this way the steel specimen gauge length is immersed in the fluid inside the disbondment. The gas mixture is bubbled through the bulk solution during the whole test to maintain the pH constant at around 6.2-6.3. Just above the top of the Perspex box ("open mouth"), a cathodic potential is applied e.g., -1.5 V versus SCE. This is measured via the reference electrode. Deep within the disbondment at the notch location the potential is measured by another reference electrode in a continuous manner throughout the tests. The pH both within the disbondment at the notch location, and in the bulk solution, was periodically monitored via use of a microelectrode. To begin the actual test, the specimen was subjected to cyclic tensile loading (triangular wave form), considering a maximum load of about 72% of the specified minimum yield strength (72% of 415 MPa).

The R value used for all experiments was set to 0.2, based on trials which showed no crack growth for higher values of 0.6 or 0.9. The cyclic loading frequency realised during the tests was 0.00064 Hz, which corresponds to a strain rate of around 1.5 X 10^{-6} s^{-1}. Each test was performed for a maximum duration of 35 days, giving about 1900 loading cycles. At the end of the test the sample was extracted and photographed following chemical cleaning to remove corrosion products. The sample was then broken open in liquid nitrogen and the fracture surface examined by SEM microscopy, determining the fracture morphology in the crack growth zone. Measurements were also made of the crack growth distance in the specimen through thickness (90° direction) and along the surface (0° direction). In this way the crack growth rate (mm/cycle), could be obtained for every specimen in two directions, considering the effect of different applied potentials at the open mouth position.

Finally, it should be noted that a key issue in the setup of the experiments was the need to recreate the potential at the NNSCC preexisting crack, that is seen in the field i.e., the zone is completely shielded from the CP, thus the potential there is the open circuit value (OCP). Thus, a considerable effort was made via trials to obtain a setup, where the measured potential at the notch was always at OCP (measured as -750 mV versus SCE), for the duration of each test. Likewise, the pH within the disbondment should be similar to the bulk value of about 6.2-6.3. From such trials it was found that OCP could be achieved when the notch position was located at least 7 cm from the open mouth (point of CP application). Furthermore, this result was obtained for a disbondment size of 5 mm (gap from bare steel surface to Perspex sleeve). Finally, to maintain the potential at the notch at OCP for the test duration (up to 35 days), it was found that a flow loop was necessary. This was achieved via the use of a peristaltic pump, pushing solution from the bulk to the disbondment, with a small flow rate of 3.5 ml/min. In addition, the test solution was occasionally refreshed i.e., once or maximum twice during each test. Without such measures, it was observed in the trials that the pH inside the disbondment would drift to values of around 11. This led in turn to the potential at the notch becoming more negative.

Figure 4 shows an example of an actual crack growth test showing the successful application of the above measures.

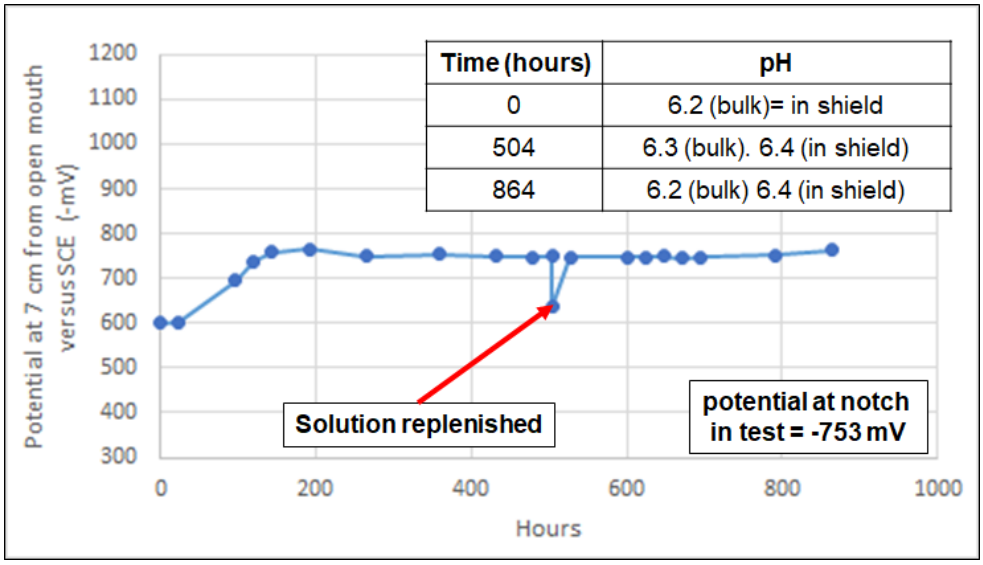

Figure 4 Monitoring of potential and pH at notch located 7 cm from site of CP application (-1200 mV versus SCE in this example with flow rate of 3.5ml/min)

As can be seen, the potential at the notch (7 cm from open mouth for all tests), was maintained at or very close to -750 mV (OCP), for the duration of the test, following initial stabilization. In addition, the pH both in the bulk and in the disbondment was maintained within a narrow range i.e., 6.2-6.4.

3. RESULTS

Crack growth was studied for several different conditions i.e., applied potentials of -1.2V and -1.5V versus SCE at the open mouth (7 cm from the notch). For comparison purposes tests were also carried out under OCP (no cathodic potential applied at the open mouth), and in air. As mentioned in the previous section, no crack growth occurred in the near neutral environment at higher R values, so all results consider the R value of 0.2.

Figure 5 below shows an example of the sample appearance after the test and after chemical cleaning.

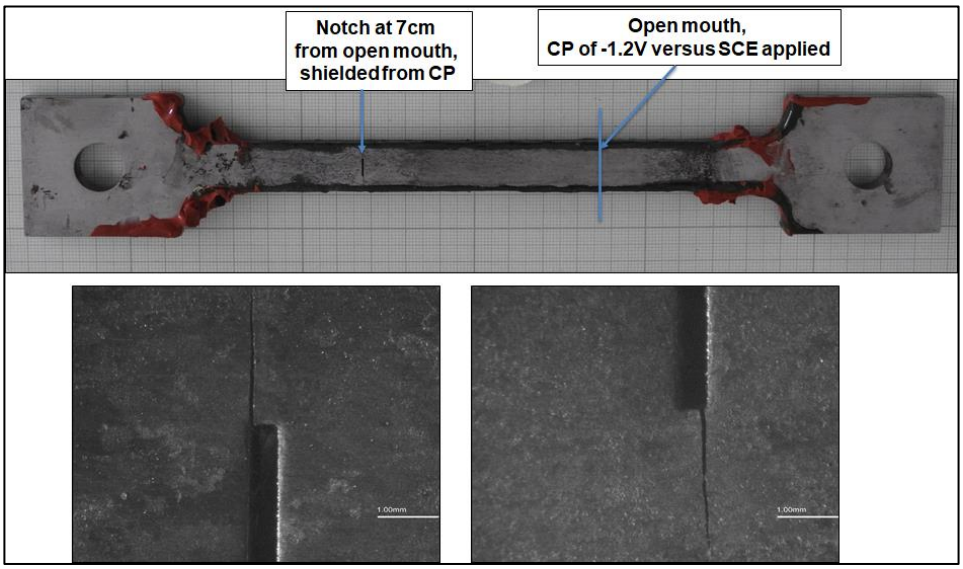

Figure 5 Visual inspection of samples post-test and after chemical cleaning. Example is for sample 6_3 (-1.2V applied at open mouth)

As can be seen, the visual inspection of the notch surface seems to suggest crack propagation during the test. Further evidence was obtained for all specimens by examination of the fracture surface, after opening in liquid nitrogen. Figure 6 shows an example of the fracture surface at low magnification for the sample 6_3.

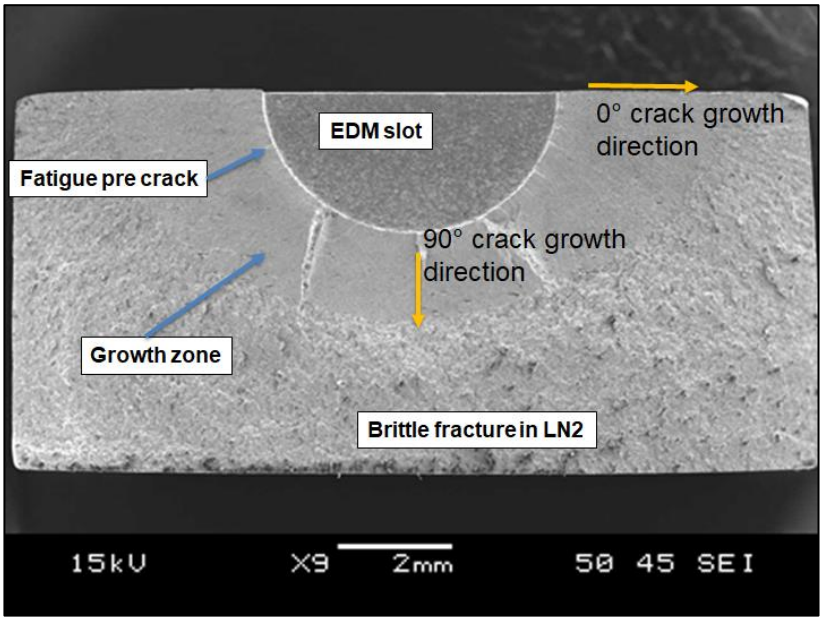

Figure 6 Examination of fracture surface via SEM at low magnification. Example is for sample 6_3 (-1.2V applied at open mouth)

Figure 6 clearly shows evidence of crack propagation during the test. For all specimens the crack growth rate was determined by measuring the crack growth (in mm), considering the through thickness direction (90°) and the surface direction also (0°). Knowing the duration of each test, the crack growth rate in mm/cycle was determined for both directions on every sample.

Figure 7 below shows representative examples of crack morphology (90° direction only) for selected conditions. Also indicated are the measured crack growth rates.

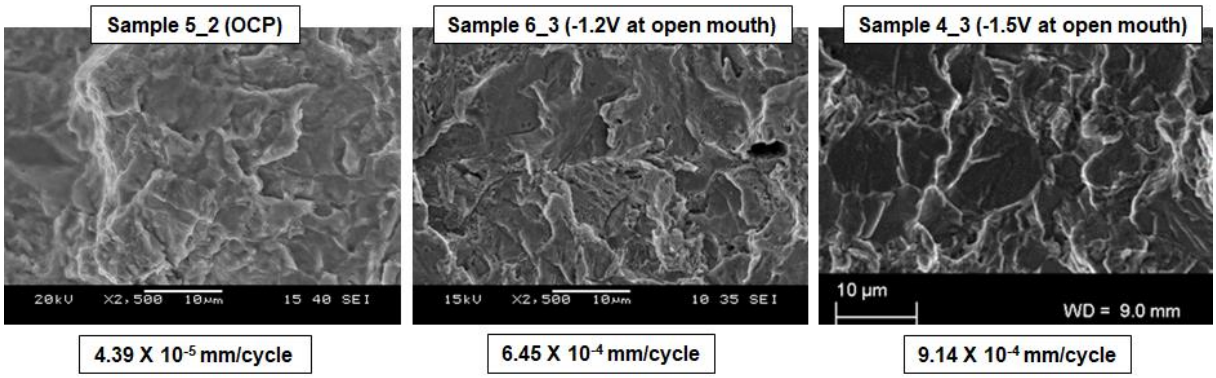

Figure 7 Fracture surfaces of selected specimens (crack propagation zone in 90° direction) after crack growth tests

As can be seen, a low crack growth rate is obtained for the sample tested with no CP at the open mouth. This is associated with a ductile fracture morphology. As the CP level far from the notch is increased, the crack growth rate is seen to increase, and is associated with an increasingly brittle-like fracture appearance.

Table 3 compares the observed crack growth rates (90° direction), for the different CP levels applied at the open mouth (7 cm from the notch), to the value obtained in air. For the comparison, the average crack growth rate for each condition (2-3 specimens) was divided by the average value in air (from 2 specimens).

Condition	Flow rate (ml/min)	(da/dN environment) / (da/dN air)
OCP (no CP at open mouth)	3.5	1.2
-1.2V versus SCE at open mouth	3.5	19.7
-1.5V versus SCE at open mouth	3.5	21.3

Table 3 Comparison of near neutral crack growth rates (90° direction) versus value in air. Note that for all tests the R value was 0.2 and the maximum load was 296 MPa

Considering the above crack growth rate ratios, it can be seen that for the OCP condition, the average growth rate was similar to that achieved in air. On the other hand, for the tests with CP applied at the open mouth, the average crack growth rate was around 20 times greater than in air.

Figure 8 shows the measured crack growth rate (90° direction), for all specimens versus the potential at 7cm distance (open mouth). Note that the OCP condition is represented by the values at the potential of -0.75V. Finally, also shown are the average growth rates based on 2 specimens for OCP and 3 specimens each for -1.2V and -1.5V.

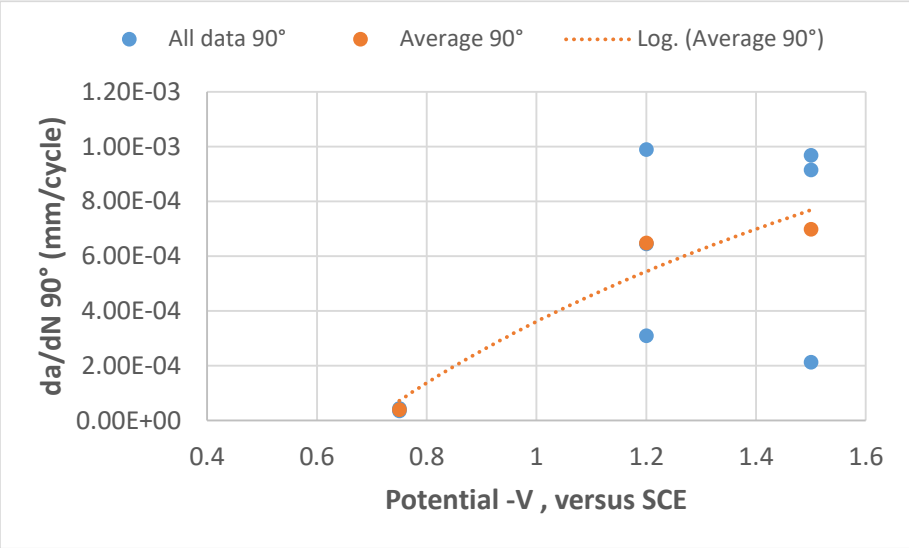

Figure 8 Effect of applied potential at open mouth on NNSCC crack growth rate (90° direction)

As can be seen, despite some scatter, the results clearly show a much higher crack growth rate when CP is present at the open mouth. Considering the average behaviour and curve, it appears that as the applied potential at the open mouth becomes more negative, the crack growth rate 7 cm away, will be increased. Comparing the average behaviour for -1.2V versus -1.5V, the crack growth rate appears slightly higher for the most negative potential.

Comparing figure 8 with specimen fracture surfaces revealed that higher growth rates were always associated with more brittle-like fracture surfaces. This was also demonstrated in figure 7.

Finally, figure 9 compares the effect of the potential at the open mouth on the average crack growth rate for both crack growth directions (90° and 0°).

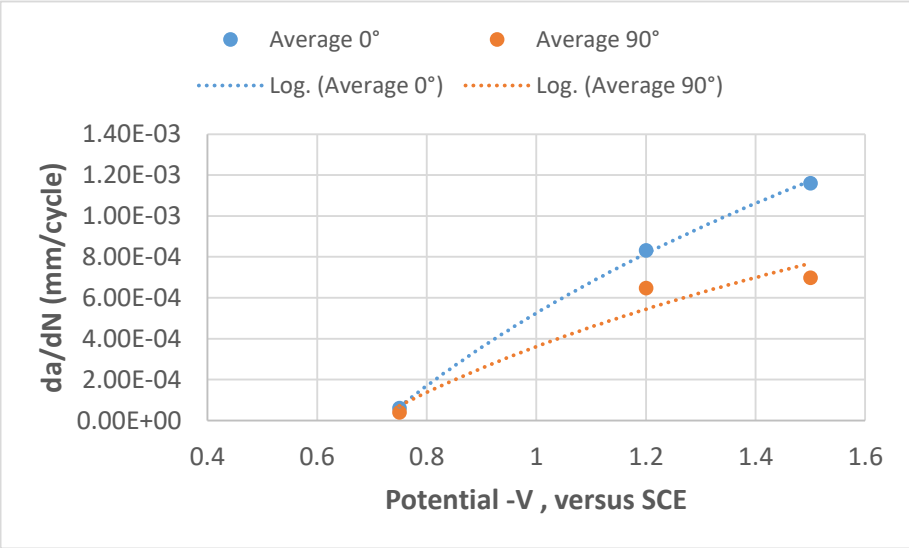

Figure 9 Effect of applied potential at open mouth on NNSCC crack growth in different directions

As can be seen, the average crack growth rate appears to be significantly faster at the surface compared to the through thickness direction, for the cases where CP was applied. For the OCP condition the same is true, although the scale on the vertical axis hides the difference.

4. DISCUSSION

4.1. Comparison with previous work

The results obtained in this study can be compared with the Canadian work carried out on an X65 grade pipe with a ferrite-pearlite microstructure, with very similar experimental setup and identical environment and the same semicircular surface flaw size [5]. To make the comparison the crack growth rates are plotted versus a combined loading factor, which takes into account the combination of the mechanical effects (stress intensity) and the environment (via loading frequency). The combined loading factor (CLF) is given by [5,6]:

$$CLF = \frac{K_{max}\Delta K^2}{f^{0.1}} \quad (1)$$

Where K_{max} is the maximum stress intensity factor, ΔK is the stress intensity range, and f is the loading frequency.

Figure 10 shows this comparison. Note that crack growth rates for the present study shown are those in the 90° direction. Those from the literature were derived from potential drop measurements. The literature crack growth rates are for samples with multiple notches i.e., located at 7.5 and 15 cm from the "open mouth" position, where the cathodic polarization was measured to be small (at 7.5 cm) or completely absent (15 cm). The plotted data thus show two points for the 7.5 cm notch and two for the notch 15 cm away from the open mouth. Finally, the figure also shows a horizontal line and vertical arrows, indicating the combined loading factor range where no crack growth was detected in the literature study i.e., 5000-6000 (MPa.m)^3/Hz$^{0.1}$.

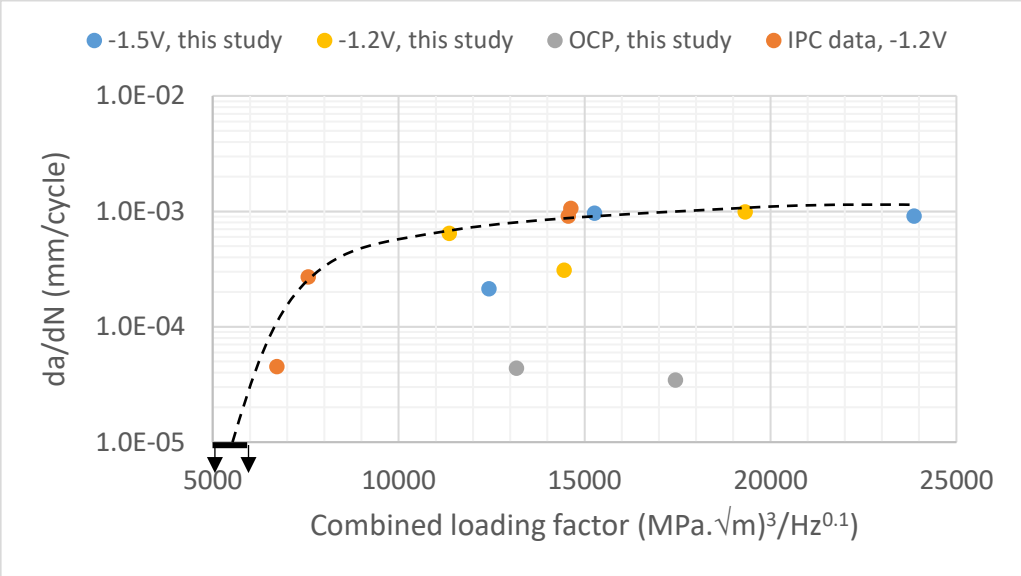

Figure 10 Comparison of crack growth rates from the current EPRG study versus previous Canadian work (IPC data) [5]

As can be seen, combining the two data sets and allowing for the existence of the threshold for crack growth, suggests that most of the data can be described by a common curve, if the two outliers from the present work are ignored (two samples with lower crack growth rates at -1.2V and -1.5V). It should

also be noted that no flow loop was used in the literature study, thus the effect of the small flow rate used in the current work does not appear to be significant.

Another important result from the current work was the very low crack growth rate seen for the case of no CP applied at the open mouth (OCP case in figure 10). In fact, from table 3, it was shown that crack growth rates under OCP conditions were found to be similar to those seen in air. This suggests a purely mechanical influenced crack growth for OCP conditions, with no effect of the environment. This surprising result differs from the literature data on NNSCC propagation where no CP was present [3,7]. Such studies on compact tension types specimens, revealed crack growth rates of 3-5 times higher for X65 steel samples tested in C2 solution, compared to the current work. The crack propagation rates observed in literature with no CP, were explained as being due to a competition between blunting (e.g., by corrosion of the crack tip), and sharpening (due to mechanical fatigue and absorbed hydrogen from general corrosion). Furthermore, by means of tests with uncoated, partially coated, and fully coated (only crack tip in contact with fluid) compact tension specimens, it was shown that crack growth rates decreased as the crack became more isolated from hydrogen generation sites. In fact, for partially or fully coated compact tension specimens, the crack growth rate was around 2.5 X 10^{-5} mm/cycle with a combined loading factor of 8600 $(MPa\sqrt{m})^3/Hz^{0.1}$. Comparison of these numbers with figure 10 appears consistent with the growth rate for the OCP case in the present study. Thus, once the difference in loading factor is taken into account, the crack growth rates fall on the same line, indicating little or no effect of the environment.

Based on the above discussion, the most likely factor influencing the low crack growth rates under OCP conditions in the present study would appear to be due to a lack of significant hydrogen accumulation at the crack tip during the test duration. This effect is tentatively suggested to be due to the smaller exposed sample surface area (one face with a small area), versus the case for uncoated compact tension specimens (up to 5 specimen faces exposed to the test solution). In addition, in the latter case, hydrogen diffusion paths from generation points on the specimen surface to the crack tip are also shorter. The overall effect could lead to a reduced hydrogen accumulation ahead of the crack tip during the OCP tests in the present study.

Finally, an additional but lesser contributing factor could be crack tip blunting. Thus, it may be, that for the shallow flaw in the current work, combined with the flow loop, that corrosion in the crack and therefore blunting of the crack tip is easier versus a compact tension specimen geometry. Thus, the shallow flaw may suffer more blunting which cannot be balanced (resharpened) by the very low level of hydrogen accumulation at the crack tip.

4.2. Main factors influencing crack growth rate

In the results section it was shown (figure 9) that an applied CP potential at the open mouth position was able to influence the crack growth rate versus no CP applied (OCP case). Moreover, in the previous section, hydrogen was suggested as the main crack driver (in synergy with mechanical fatigue), based on literature arguments. For hydrogen generated via CP far from the crack tip to play a role, long range diffusion of hydrogen to the notch position is required. This requirement is analysed below.
To evaluate the hydrogen diffusion from the open mouth to the notch (70 mm distance), a diffusion coefficient is required. From literature, a range was found (9.33 - 17.00 X 10^{-10} m^2/s) considering a similar strength level (X65) and appropriate microstructure (ferrite-pearlite) [8,9]. Using these extremes, the hydrogen concentration profile along the length of the specimen was determined via use of a finite element framework in 3D. Note that it was assumed in the simulations that hydrogen could not diffuse out of the sample. An example of a result is shown in figure 11 below. Note that the results are shown in terms of relative concentration i.e., local concentration divided by the surface value.

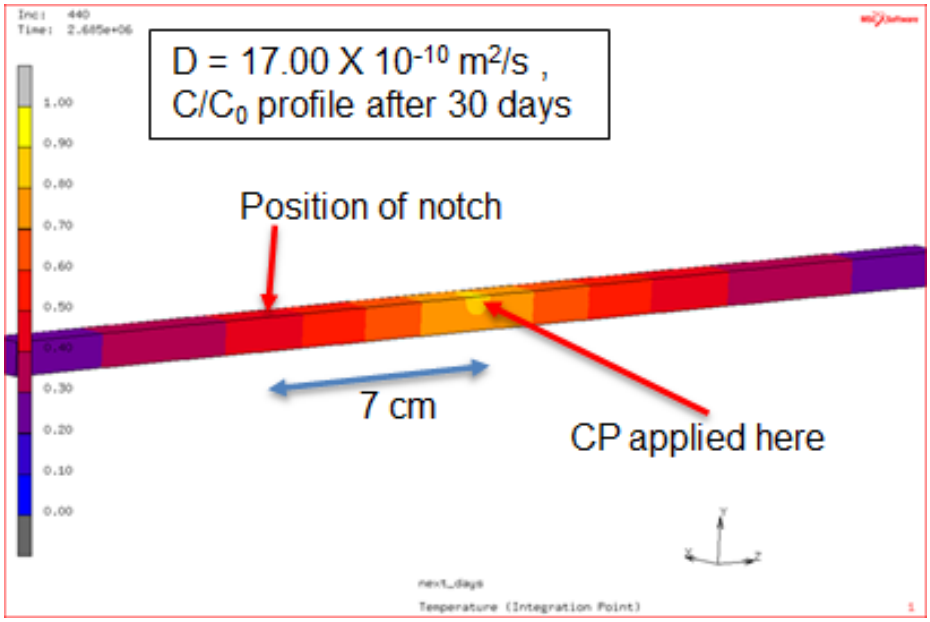

Figure 11 Calculated hydrogen concentration along tensile specimen from open mouth position towards notch

As can be seen, after 30 days duration, significant hydrogen penetration within the specimen has occurred. Thus even 12 cm away from the open mouth (CP application zone), around 20% of the surface concentration at open mouth has diffused. Figure 12 shows concentration profiles for the two diffusion coefficients, considering the test duration of 30 days.

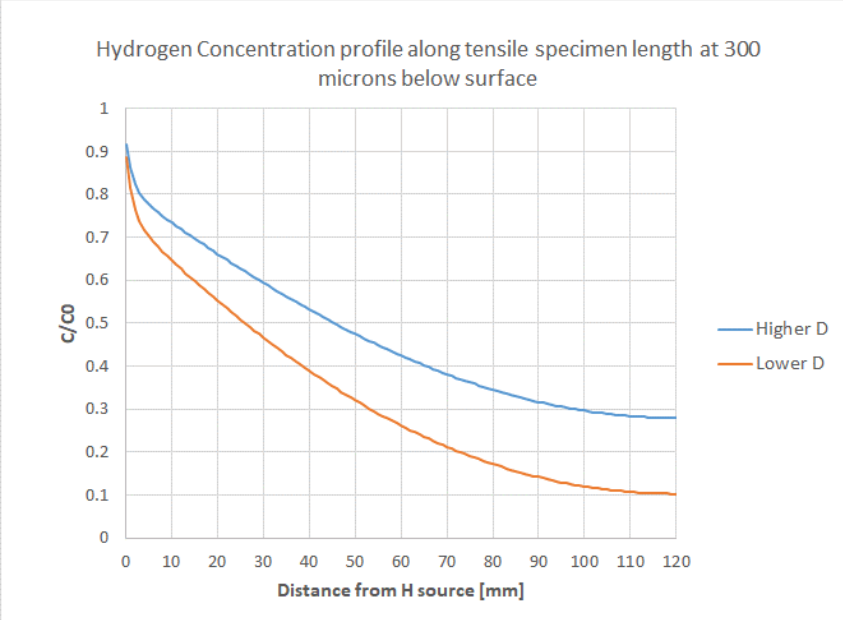

Figure 12 Hydrogen concentration versus distance from open mouth (along specimen length) for two diffusion coefficients considering a time of 30 days

From figure 12, considering 70 mm between open mouth and notch location, around 20-40% of the hydrogen generated at the open mouth could diffuse to the notch within the 30 days testing time. Thus, this result shows that hydrogen generated from CP at the open mouth can diffuse to the crack site during the test duration. Moreover, it should be remembered that the potential between the open mouth and notch location (along the disbondment) decays to the OCP value. Measurements of the potential showed that when applying -1.5V (SCE) at the open mouth, a cathodic potential of -1.0V was

observed at 5 cm distance from the notch and -0.90 V at 4.5 cm. Thus, considering these significant cathodic potentials (i.e. much more negative) versus the theoretical (thermodynamic) threshold value (-0.66V SCE) needed for hydrogen generation [5], the actual diffusion distance for hydrogen to reach the crack tip may be a bit shorter than the 7 cm considered in these calculations.

4.3. Modelling crack growth kinetics

In the previous sections the key role of hydrogen on crack growth kinetics was demonstrated. In literature NNSCC crack growth kinetics derived from compact tension specimens for a range of environments without CP applied, has been shown by Chen et al., [3] to be proportional to the combined loading factor shown in equation (1). In this approach, above some threshold for crack growth, the crack growth rate in fatigue (da/dN), is proportional to a mechanical fatigue loading term ($\Delta K^2 K_{max}$)and a loading frequency term ($f^{-0.1}$)representing corrosion effects. Building on this approach, Lu et al [10] examined a range of NNSCC data from literature (no CP applied), finding that the fatigue crack growth rate (da/dN) for compact tension specimens could be described by:

$$\frac{da}{dN} = B(K_{max}\Delta K^2 f^{-0.1})^p \quad (2)$$

Where p was found to take a value of $p = 2$. The parameter B depends on the environment and material. By considering a model where crack growth rate depends on the distance between the fracture process zone ahead of the crack and the crack tip (r_{FPZ}), the authors derived the following expressions:

$$\frac{da}{dN} \propto \left[ln\left(\frac{C_{CR}}{C_0}\right)\right]^{-2} K_{max}^2 \quad (3)$$

$$B = B_0\left[ln\left(\frac{C_{CR}}{C_0}\right)\right]^{-2} \quad (4)$$

In this approach the crack growth depends on the ratio of the hydrogen concentration (C_0) absorbed into the steel bulk (from corrosion reactions or via CP), versus some critical hydrogen concentration at the fracture process zone (C_{CR}). It is also assumed the diffusion of hydrogen in the steel bulk to the fracture process zone is not rate limiting. The crack growth rate also depends on the parameter B_0 , which presumably reflects the role of the material. Finally, to obtain values of C_0, the authors used experimental literature data where this parameter was measured for different pH values and potentials. The following equation was derived for a pH of 6.3 (relevant for the current study) [10]:

$$C_0 = 10^{-6}\frac{(5+10V)\times 10^{-10} exp\left(-\frac{V}{0.03}\right)}{5+10V-10^{-10} exp\left(-\frac{V}{0.03}\right)} \quad (5)$$

Where the units of concentration are mol/cm^3, and the potential V in volts is versus CSE.

Using equations (2), (4) and (5) with $p = 2$, Lu et al [10] were able to fit a range of experimental data (compact tension specimens under open circuit potential with solution different pH), using a single set of fitting parameters i.e., B_0 = 1.9 X 10^{-13} MPa^{-6}m^{-2}s$^{-0.2}$ and C_{CR} = 4193 ppm. The physical meaning of the critical concentration and its fitted value was not explained in the reference. Also, since the critical concentration is related to r_{FPZ} in the paper, it should lead to realistic values of the latter parameter also. However, this was not examined by Lu et al.

The above modelling approach was applied to the data generated in the current study (-1.2V and -1.5V SCE), considering data for both cracking directions (0 and 90°). To add data at more positive potentials, the work of Chen et al [3] was used (-0.75V SCE with the same C2 solution using compact tension specimens). Initial fitting of equation (2) to these 3 conditions revealed a poor fit to the data from the

present work. On the other hand, an excellent fit was obtained when p was fixed to p = 1, with a reduced but acceptable fit for the literature data. However, since *p* was found to be equal to 1, equation (4) can no longer be derived. Thus, it was decided to use a "practical" approach to derive a simple relationship between B in equation (2) and the hydrogen concentration values from equation (5). This exercise led to the following relationship between the fitted values of *B* and C_0 from equation (5):

$$B = 1.03 \times 10^{-11} ln(C_0) + 4.76 \times 10^{-11} \quad (6)$$

Table 4 compares the original fitted values of *B* (applying equation (2) to the data with p = 1), to calculated values of *B*, from equation (6). Also shown are the relevant C_0 values:

Solution	Potential versus SCE (V)	C_0 (ppmw)	B from experiments ($MPa^{-3}m^{-0.5}s^{-0.1}$)	B from equation (6) ($MPa^{-3}m^{-0.5}s^{-0.1}$)
C2 (pH = 6.3)	-0.75 (Work of Chen et al)	0.39	3.86×10^{-11}	3.80×10^{-11}
C2 (pH = 6.3)	-1.2 (this work)	0.98	4.51×10^{-11}	4.74×10^{-11}
C2 (pH = 6.3)	-1.5 (this work)	1.36	5.25×10^{-11}	5.08×10^{-11}

Table 4 Comparison of experimentally obtained *B* values with C_0 and predictions from equation (6)

From table 4 it can be seen that the fitted values of B using equation (2) and p = 1, depend on C_0. Thus, as C_0 is increased *B* values are higher. This result confirms that the experimental crack growth rates increase with absorbed hydrogen content. Secondly, table 4 shows that the simple model for *B* i.e., equation (6), fits the data very well. The new "practical" model incorporating the effect of absorbed atomic hydrogen on crack growth kinetics, is now given by combining equations (2) and (6):

$$\frac{da}{dN} = [1.03 \times 10^{-11} ln(C_0) + 4.76 \times 10^{-11}][K_{max} \Delta K^2 f^{-0.1}] \quad (7)$$

Where C_0 is given by equation (5). Note that this model assumes that hydrogen diffusion to the crack tip is not rate limiting.

Figures 13 and 14 shows the application of the new model i.e. equation (7), to the experimental crack growth data from this study and from literature.

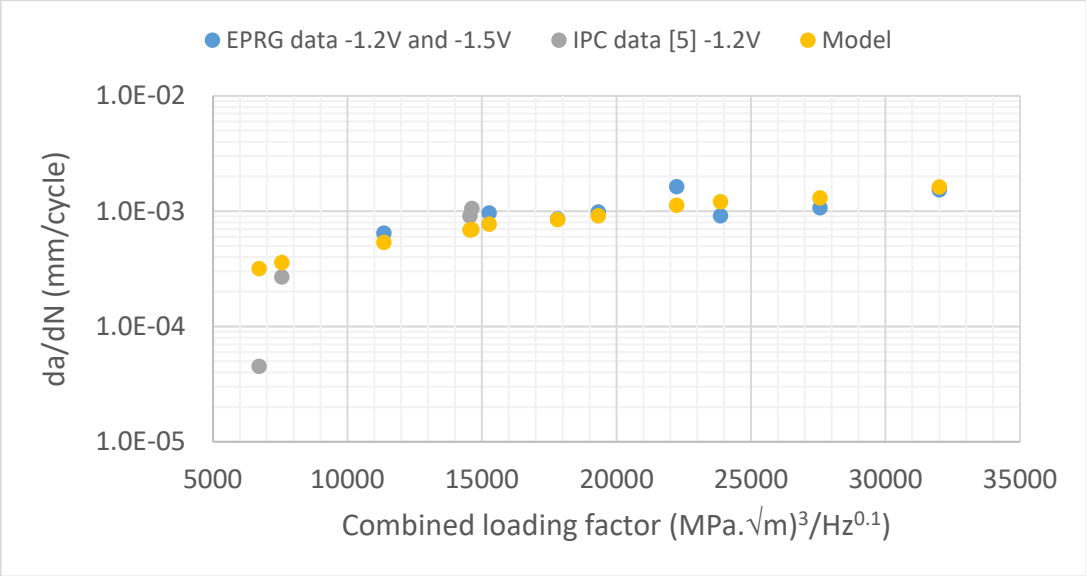

Figure 13 Comparison of experimental crack growth rates in C2 solution (present EPRG data and data from reference [5]) with the crack growth model in equation (7).

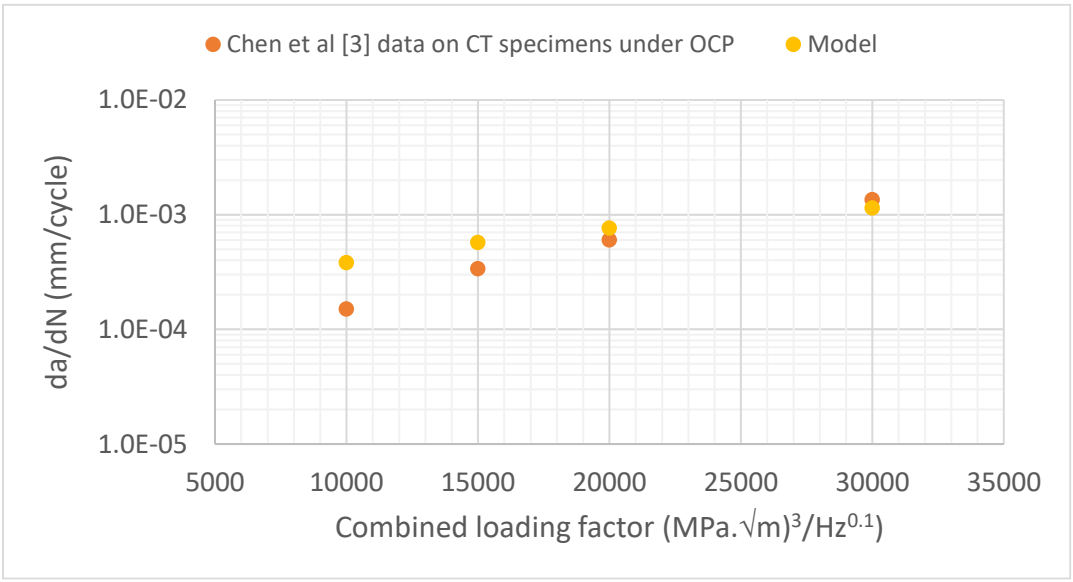

Figure 14 Comparison of experimental crack growth rates from reference [3] with the model in equation (7). Test solution is C2, and potential is -0.75V SCE

As can be seen from figure 13, the fitted model provides very good agreement for the EPRG dataset. In addition, the model provides good predictions when compared to literature data (IPC data) obtained on a very similar type of specimen with the shallow surface crack [5]. As expected, at low combined loading factors around 6700 $(MPa.\sqrt{m})^3Hz^{-0.1}$, i.e., near the threshold of 5000-6000 identified in figure 10, the model overestimates crack growth rates. The model predictions in figure 12 also provide excellent agreement for surface crack growth direction (0°) data from the present work (corresponding to half of the data points labelled EPRG data). This shows that the higher crack growth rates in the 0° direction versus 90° in figure 9, can be explained solely by differences in local mechanical driving force i.e., higher stress intensity at the surface versus the through thickness.

Figure 14 shows reasonable agreement between the model and the literature data at OCP for compact tension samples. Thus, at more positive potentials where lower hydrogen levels are present, the model is able to give a reasonable prediction for a range of combined loading factors.

Finally, figure 15 illustrates the model trends considering the effect of potential and combined loading factor.

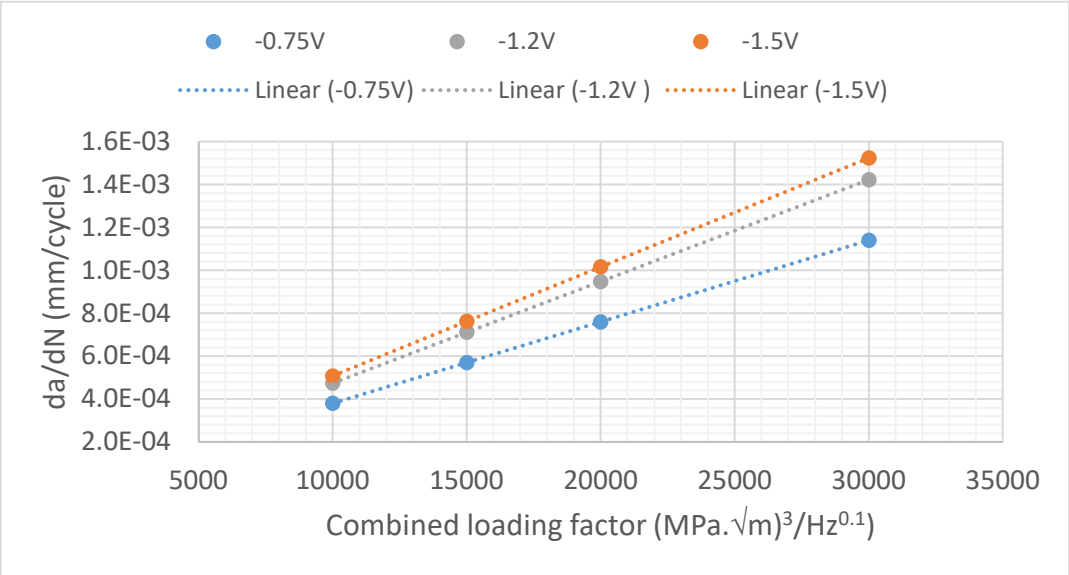

Figure 15 Illustration of model predictions from equation (7) over a wide range of potentials and mechanical loading factors. Note that frequency is fixed at that of the present tests = 0.00064 Hz.

As can be seen, equation (7) gives physically realistic trends i.e., lowering the potential provides more hydrogen which enhances crack growth. In addition, it can clearly be seen the enhancing effect of the mechanical driving force. Thus, at high values of the combined loading factor, the effect of increasing hydrogen content (lowering potential) on crack growth rate is stronger.

5. CONCLUSIONS

In this work the effect of cathodic protection (CP) on near neutral stress corrosion crack growth (NNSCC) in X60 grade pipe, has been studied by means of laboratory scale crack growth tests on tensile specimens with shallow cracks. Tests were performed using a synthetic soil solution (C2). The setup included a 5mm thick disbondment where different CP levels were applied at the open mouth but was locally absent at the crack site located 7 cm away. From the results obtained, the following conclusions have been drawn:

- Low crack growth rates (comparable to tests in air and with ductile fracture surface) were observed for samples tested with no CP applied at the open mouth (OCP case).

- Increasing the CP level at the open mouth (i.e., applying -1.2V and -1.5V versus SCE) led to a remarkable increase in crack growth rate in the distant shielded zone, roughly 20 times higher than that seen in air. Such samples revealed a more brittle-like fracture surface.

- Comparison of the crack growth rates with literature data with a very similar experimental setup and crack geometry revealed good agreement for the same CP level at open mouth, once differences in mechanical loading factor were taken into account.

- For the OCP case the low crack growth rates contrasted to that seen in literature i.e., using compact tension specimens crack growth rates were 3-5 times higher in the same solution.

- The low crack growth rates for the OCP case were tentatively suggested to be mainly due to the difference in specimen geometries i.e., small exposed specimen surface area and longer diffusion paths for the specimen used in the current work. This could lead to a lower concentration of hydrogen being present at the crack tip during the test versus the compact tension specimen case.

- The experimental results and modelling work in the present study suggest crack growth was driven by hydrogen (effect of CP at the open mouth) and mechanical fatigue. Hydrogen diffusion calculations supported these results i.e., proving that long range bulk diffusion of a significant quantity hydrogen from the open mouth zone to the crack site was feasible during the test duration of 30 days.

- A practical model for the crack growth rate was developed from the current experimental data and literature data on compact tension specimens:

- $\frac{da}{dN} = [1.03 \times 10^{-11} ln(C_0) + 4.76 \times 10^{-11}][K_{max} \Delta K^2 f^{-0.1}]$.

- The developed model considered that crack growth rate was driven by the absorbed hydrogen content from corrosion reactions or CP, as well as by mechanical loading effects.

- The practical model provided good agreement with the experimental data and literature data considering a wide range of combined loading factors and potential levels (-0.75 to -1.5V SCE).

6. REFERENCES

1. W. Chen and J. Luo, Corrosion, Vol. 60, No. 8, (2004), p. 778-786.
2. B. Williams, S. Lambert, R. Sutherby and A. Plumtree, Corrosion, Vol. 60, (2004), p. 95-103.
3. W. Chen and R. Sutherby, Met. Mater. Trans. A, Vol. 38A, (2007), p. 1260-1268.
4. B. Gu, J. Luo and X. Mao, Corrosion, Vol. 55, (1999), p. 96-106.
5. A. Egbewande, A. Eslami, W. Chen, R. Worthington, R. Kania and G. Van Boven, IPC2010, paper No. 31436.
6. A. Egbewande, W. Chen, R. Eadie, R. Kania, G. Van Boven, R. Worthingham, and J. Been, Corrosion Sci., Vol. 83, (2014), p. 343-354.
7. J. Been, R. Eadie and R. Sutherby, IPC2006, paper No. 10345.
8. G. Park, S. Koh, H. Jung and K. Kim, Corrosion Sci., Vol. 50, (2008), p. 1865.
9. J. Kittel, V. Smanio, M. Fregonese, L. Garnier and X. Lefebvre, Corrosion Sci., Vol. 52, (2010), p. 1386
10. B. Lu, F. Song, M. Gao and M. Elboujdaini, NACE Corrosion (2012), paper No. 01152.